RESEARCH ARTICLE

NANO · MICRO small
www.small-journal.com

# Asymmetric Microgels with Tunable Morphologies by Assembly-Guided Polymerization of Liquid Crystalline Monomers

*Nadja A. Wolter, Hannah Küttner, Jonas Schmitz, Matthias Karg, and Andrij Pich**

**Understanding and controlling the morphology of microgels is crucial for optimizing their properties and functions in diverse areas of application. The fabrication of microgels that exhibit both structural and chemical anisotropy using a template-free approach faces significant challenges. Existing approaches toward such microgels are typically limited to templating methods with low throughput. Here, an alternative bottom-up approach is developed for producing non-spherical *N*-vinylcaprolactam (VCL) based microgels through semi-batch precipitation polymerization, incorporating a functional comonomer with a liquid crystalline (LC) moiety. 4-methoxybenzoic acid 4-(6-acryloyloxy-hexyloxy)phenyl ester (LCM) is used as the LC comonomer. The resulting morphology of those microgels is tuned to multilobe-, dumbbell-, and raspberry-like shapes. The different morphologies are obtained by varying the addition time of LCM, temperature, solvent ratio, and monomer ratio. The microgel morphologies are characterized by (cryogenic) transmission and scanning electron microscopy. The thermoresponsiveness is investigated by dynamic light scattering (DLS), while the incorporation of LCM into the microgel structure is determined via $^{1}$H-NMR and Raman spectroscopy. The experimental data indicate that adjusting reaction conditions enables the fabrication of microgels with various morphologies. Finally, their capability to solubilize hydrophobic substances is demonstrated by successfully facilitating the uptake of the hydrophobic dye Nile Red (NR).**

## 1. Introduction

Internal morphology is an essential property of polymeric colloids that has attracted growing interest in the soft matter community over the past decades. Asymmetric, anisotropic, and multicompartment particles show interesting properties for applications in the fields of interface chemistry, material science, and applied optics.[1–5] Morphology-related design strategies are often inspired by colloidal structures that can be found in nature. In biological systems, the formation of complex structures is based on supramolecular interactions such as hydrogen bonding, hydrophobic, and electrostatic interactions, and aromatic stacking.[6]

Microgels are a promising class of soft matter as they consist of soft cross-linked colloidal polymer networks, which have increasingly gained attention because of their versatile fields of applications.[7] They are of particular interest within the field of smart polymeric materials as their physicochemical properties can be altered by numerous external stimuli such as temperature,[8–10] pH,[11] ionic strength,[12] light,[13] or solvent composition.[14] These stimuli-responsive materials demonstrate huge potential in various applications, including catalysis,[15] drug delivery processes,[16,17] and surface coatings,[18,19] which makes them attractive candidates across diverse fields such as nanotechnology and medicine.[20,21] Incorporating functional comonomers into these microgels allows for tailor-made responsivity and broadens the field of applications. For example, spherical microgels based on *N*-vinylcaprolactam (VCL) are temperature-responsive as they exhibit a temperature-induced volume-phase transition (VPT) at ≈32 °C in water.[22] In addition, their

N. A. Wolter, H. Küttner, A. Pich
Institute of Technical and Macromolecular Chemistry
RWTH Aachen University
Wendlingweg 2, 52074 Aachen, Germany
E-mail: pich@dwi.rwth-aachen.de

The ORCID identification number(s) for the author(s) of this article can be found under https://doi.org/10.1002/smll.202410502



DOI: 10.1002/smll.202410502

N. A. Wolter, H. Küttner, A. Pich
DWI – Leibniz Institute for Interactive Materials
Forckenbeckstraße 50, 52074 Aachen, Germany

J. Schmitz, M. Karg
Institute for Physical Chemistry
Heinrich-Heine-University Düsseldorf
Universitätsstr. 1, 40225 Düsseldorf, Germany

A. Pich
Aachen-Maastricht Institute for Biobased Materials (AMIBM)
Maastricht University
Brightlands Chemelot Campus
Urmonderbaan 22, Geleen 6167 RD, The Netherlands

biocompatibility makes them particularly interesting for medical and biological applications.[23–25]

Microgels with spherical morphologies can be easily and efficiently produced using precipitation or emulsion polymerization.[26] However, synthesizing microgels with non-spherical morphologies is more complex and often limited to low throughput techniques. Most of these approaches are bottom-up template-based strategies such as microfluidics or particle replication in nonwetting templates (PRINT).[27–30] For example, droplet-based microfluidics was applied to synthesize microgels with rod-shaped morphologies using a special microfluidic chip and an on-chip gelation technique.[31] Complex morphologies can also be realized via top-down methods such as lithography. Stop-flow-lithography has been used to fabricate complex shapes such as microgels with a snowflake morphology.[32]

However, there are only limited approaches of template-free bottom-up synthesis methods for the generation of non-spherical microgels. Our group recently developed a novel strategy for synthesizing asymmetric microgels by the assembly-guided polymerization of functional monomers. Supramolecular self-assembly and polymerization of pyrazole-modified monomers were used to induce microgels with non-spherical shapes.[33] Another approach is based on the coacervation of oppositely charged ionizable groups for the generation of polyampholyte Janus-like microgels.[34]

Shape plays a significant role in the behavior and functionality of polymeric particles as the geometry of these particles influences their physical, chemical, and biological interactions, which are critical in fields like drug delivery.[35] Evidence suggests that particle shape significantly influences their fundamental function, such as degradation for the release of therapeutic drugs.[36,37] For example, non-spherical particles with varying thicknesses may exhibit unique degradation profiles, as their shape dynamically evolves over time. Furthermore, the transport of particles, e.g., in the body, is highly affected by shape. As the movement of spherical particles is predicted more easily, asymmetric particles move in a more complex way and may align or tumble in the presence of a flow.[35,36] Non-spherical particles with multiple compartments are excellent candidates for unique container systems. For example, many drugs are rather hydrophobic and, therefore, insoluble in aqueous media, making them not accessible for uptake in many conventional microgels. This issue can be addressed by tailoring the hydrophilicity and hydrophobicity of microgels through the incorporation of hydrophobic comonomers and creating inhomogeneous structures with hydrophobic compartments within the polymer network.[38,39]

Among the classes of soft materials, liquid crystals (LCs) are a unique class of stimuli-responsive soft matter. LCs have the ability to self-organize depending on external stimuli such as temperature, light, or magnetic fields.[40,41] The liquid crystalline (LC) phase is a distinct phase that arises between the crystalline solid state and the isotropic liquid state. LCs are classified into two categories: thermotropic and lyotropic. Thermotropic LCs are fluid phases in which the anisotropic molecule parts, the mesogens, exhibit long-range orientational order that occurs as a function of temperature variation. For the preparation of LC polymeric networks, the mesogenes are equipped with flexible spacers and polymerizable units, such as epoxy-, acrylate- or methacrylate groups.[42] Such LC monomers are used for the preparation of polymer films,[43–47] gels[48] or particles.[49–53] Martella et al. prepared LC polymer films that show temperature-triggered self-curving behavior, which depends on the length of flexible spacers and the orientation of the esters in the aromatic mesogen.[46] Shaha et al. showed the preparation of LC polymer films that can change their shape close to the human body-temperature.[54] However, there are only limited examples of LC polymer particles that can be generated using conventional polymerization techniques such as suspension-,[51] dispersion-,[55,56] or precipitation polymerization.[57] Schenning et al. reported the preparation of cross-linked LC particles using conventional precipitation polymerization.[49] The same group reported the preparation of shape-changing LC particles using thiol-ene dispersion polymerization. To generate the reversible shape, the particles had to be embedded in a polyvinyl alcohol film, followed by mechanical stretching and photopolymerization.[58] There are only very few examples of LCs that have been used in combination with microgels.[59,60]

In this work, we present an alternative bottom-up approach toward the design of asymmetric microgels with different non-spherical morphologies using a template-free semi-batch precipitation polymerization approach using LC monomers. We chose VCL as a temperature-responsive hydrophilic monomer and 4-methoxybenzoic acid 4-(6-acryloyloxy-hexyloxy)phenyl ester (LCM) as a hydrophobic LC monomer. To overcome the insolubility of LCM, dimethyl sulfoxide (DMSO) was chosen as an organic co-solvent as it is an extremely versatile organic solvent that is used in pharmaceutical synthesis and drug delivery processes in the body and is miscible with water.[61] Our experimental data suggest that the morphology of the microgels and formation of the LC domains is influenced by the amount and addition strategy of LCM during the synthesis. Furthermore, changing the reaction temperature could also affect the shape of the microgels. The microgels were afterward loaded with the hydrophobic model substance Nile Red, investigating the potential of those microgels as container systems for hydrophobic substances.

## 2. Results and Discussion

### 2.1. Chemical Composition

The objective of this work was to control the morphology of microgels by using a liquid crystalline (LC) monomer capable of assembly and copolymerization with *N*-vinylcaprolactam (VCL) in a surfactant-free precipitation polymerization. The copolymerization was performed in the presence of the initiator 2,2′-azobis(2-methylpropionamidine) dihydrochloride (AMPA) and the cross-linking agent *N*,*N*′-methylenebis(acrylamide) (BIS). To introduce the LC domains, 4-methoxybenzoic acid 4-(6-acryloyloxy hexyloxy)phenyl ester (LCM) was selected since it is a widely explored monomer for the preparation of liquid crystalline networks (LCNs).[47,62,63] LCM melts at 55 °C where it transforms into the isotopic phase. Below 44 °C, it changes into a monotropic nematic phase and can remain in this phase even at room temperature before crystallization after a few hours.[46] Due to its high hydrophobicity and, therefore, insolubility in water, semi-batch synthesis was chosen, and LCM was pre-dissolved in DMSO as a water-miscible organic solvent. (**Figure 1**). The ratio of VCL

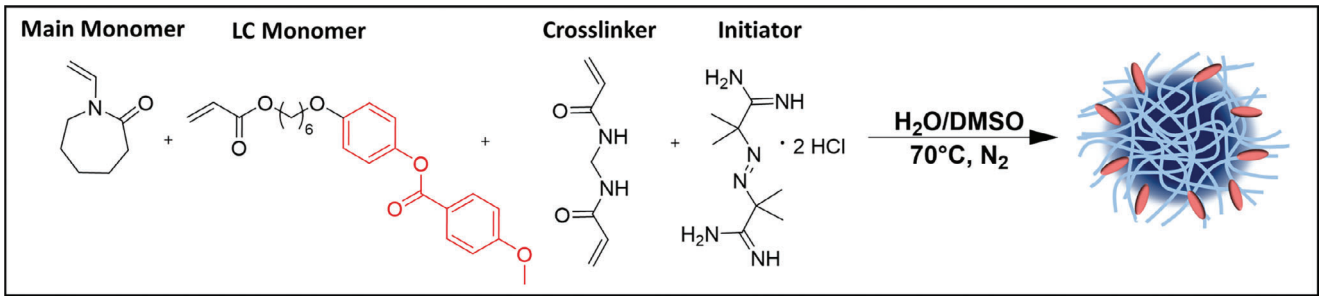


**Figure 1.** Synthesis scheme for pVCL microgels with LC domains.

to LCM was set between 100:0 and 70:0 with a concentration of 0.16 mmol $mL^{-1}$. The amount of AMPA and BIS was set to 0.2 and 1.3 mol%, respectively, in regard to the total monomer content. In conventional microgel synthesis, the amount of initiator is higher and can range, for example, from 0.6 to 1.2 mol%.[64,65] We chose to decrease the amount to 0.2 mol%, which results in the formation of fewer radical centers, which promotes the formation of larger microgels as described in previous works.[66] The cross-linker quantity was reduced in relation to conventional microgel synthesis, resulting in a loosely cross-linked microgel network. We hypothesize that the resulting high network flexibility supports the self-assembly of the mesogens between the LCM molecules, leading to the formation of LC domains.

The yield of the microgels was determined from the lyophilization of the dialyzed microgels and can be found in the Supporting Information (Tables S1, S3 and S5, Supporting Information). NMR and Raman studies were performed to determine the chemical composition of the microgels that were obtained. The $^1$H-NMR spectra of the p(VCL-*co*-LCM) microgel prove the successful copolymerization of LCM due to the broadening of the aromatic signals from LCM between 6.5 and 8.5 ppm and the disappearing of the signals between 5.5 and 6.5 ppm that can be assigned to the polymerizable vinyl group of the LCM (**Figure 2**a). The efficient incorporation of LCM by copolymerization was also validated via Raman spectroscopy (Figure 2b,c), where the pVCL microgel is indicated by the black line, while the red line indicates the p(VCL-co-LCM) microgel. The magnified section of the Raman spectra in Figure 2c shows the carbonyl stretching vibrations at 1624 $cm^{-1}$ from the VCL-amide. The p(VCL-*co*-LCM) microgel has additional signals at 1728 and 1607 $cm^{-1}$ caused by the carbonyl stretching vibrations and the aromatic C═C stretching vibrations of LCM, respectively.

### 2.2. Influence of the Addition Time of LCM on the Microgel Morphology

To determine a suitable addition time of LCM to the polymerization mixture, the synthesis of pure pVCL microgels was monitored by real-time reaction calorimetry, detecting the heat generation rate (qr_rtc) and the turbidity during the reaction (**Figure 3**a). Both the heat generation profile and the turbidity evolution indicate that the polymerization of VCL cross-linked with BIS was completed within 20 min, which is in accordance with the literature where the synthesis has been performed with slightly different initiator and cross-linker compositions.[67] Therefore, only a time within the first 20 min is suitable for the addition of LCM. Integrating the heat generation rate curves results in the thermal conversion, providing insights into the percent consumption of VCL and BIS during the synthesis. Since BIS is present only in minor amounts as a cross-linker, it was omitted from the further analysis and comparison of thermal conversion. After 2 and 3 min, VCL conversion reaches only 10% and 18%, respectively. However, after 4 min, 28% of VCL is converted, increasing to 40% after 5 min and 89% after 10 min. Since DMSO was used as a co-solvent, reaction calorimetry with 10 v% DMSO was performed to investigate how the reaction time is affected. After 2 min, VCL conversion reaches 8%, which is comparable to the synthesis conducted without DMSO. However, after 3, 4, and 5 min, only 13%, 20%, and 27% of VCL are converted, respectively, with a conversion of 68% observed after 10 min. The presence of DMSO during the synthesis shows a retarding effect on the heat generation rate, and the turbidity is lowered compared to the reaction without DMSO. A series of semi-batch syntheses were performed by varying the delay time at which LCM was added to the polymerization mixture post-initiation. cross-linker, initiator, and monomer compositions remained constant using a 95:5 ratio of VCL to LCM. The DMSO/water ratio of 5 v% DMSO was selected to minimize the DMSO content during the synthesis. After purification by dialysis against water, the morphologies of the microgels were examined by transmission electron microscopy (TEM). Figure 3c–i shows TEM images of p(VCL-*co*-LCM) microgels with LCM additions between 0 to 10 min post-initiation and pure pVCL microgels for comparison (Figure 3b). All images show the successful synthesis of monodisperse spherical microgels. When adding LCM simultaneously as the initiator without delay, the microgels show no defined structural changes according to TEM images. However, the core of the microgels shows a higher contrast relative to the corona. In the TEM image from pure pVCL microgels, the core is also visible, though there is a slightly reduced contrast difference between the core and corona. The darker core results from the preferential reaction between VCL and BIS rather than VCL with itself. This is supported by the heat generation profile (Figure 3a) and established reaction kinetics, as well as quantum mechanical calculations in the literature, leading to a denser cross-linking within the core.[67]

The microgels obtained after LCM addition time of 2 min exhibit, in addition to a dark core region, small compartments surrounding the core that display higher contrast compared to the rest of the microgel (Figure 3d). The differences in contrast arise from variations in electron density in the microgel. In the LCM-rich regions, where polymer chains are highly ordered, the

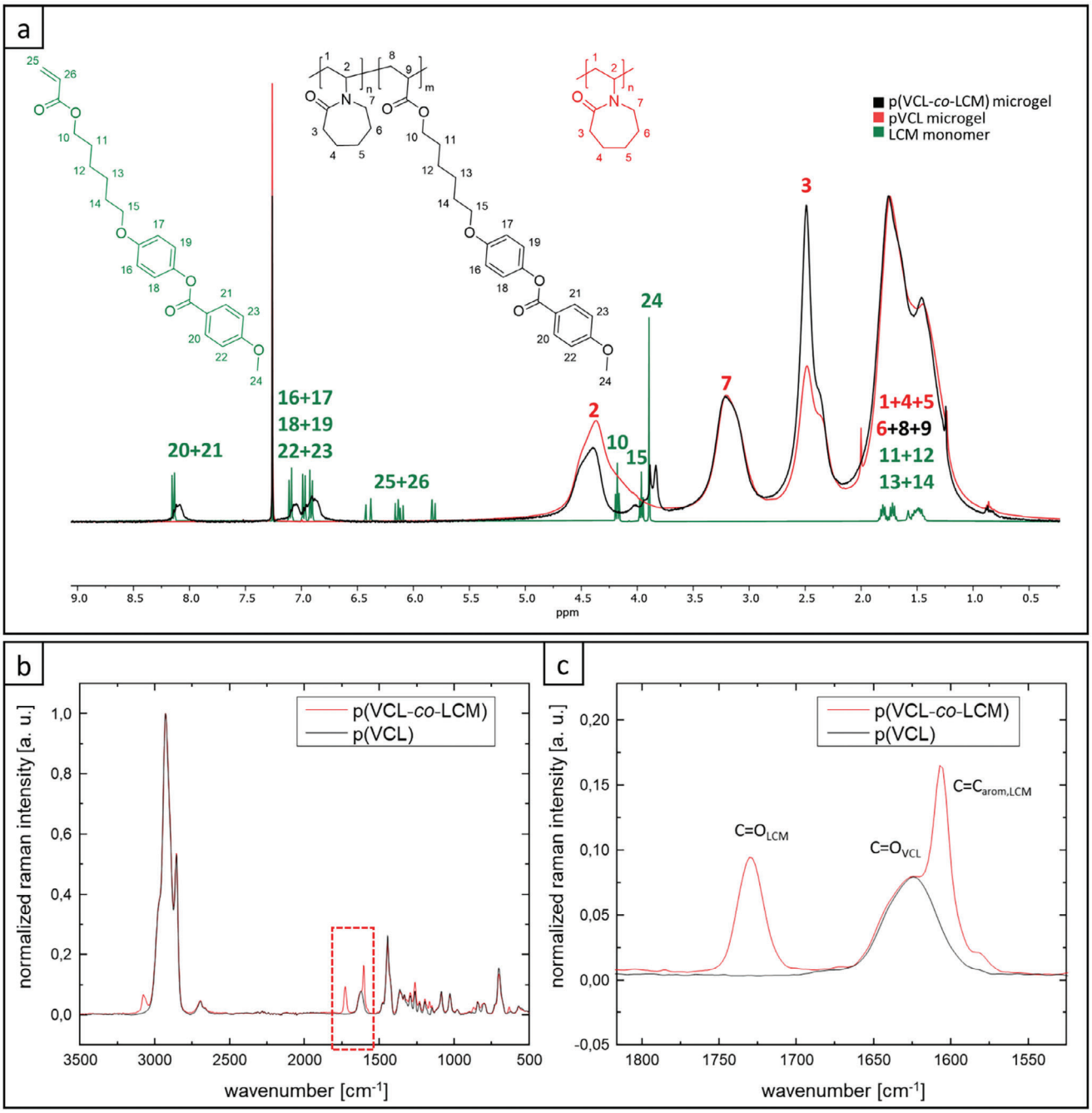


**Figure 2.** a) $^{1}$H-NMR spectra of LCM (green), pVCL microgel (red), and p(VCL-*co*-LCM) microgel (black) in $CDCl_3$ showing the successful incorporation of LCM into the microgel; b,c) Raman spectra of pVCL (black) and p(VCL-*co*-LCM) microgels (red) measured between 500 and 3500 $cm^{-1}$. For p(VCL-*co*-LCM) microgels, a ratio of 95:5 of VCL to LCM was used.

electron density is higher compared to the loose, amorphous regions of the rest of the microgel. Generally, regions with higher density scatter more electrons and, therefore, appear darker than low-density regions.[68] As there are no significant differences in atomic number between the elements of the two monomers, the results indicate that the dark compartments arise from differences in density and crystallinity compared to the rest of the microgel. The compartment formation and darker core region can be attributed to the hydrophobicity and self-alignment properties of the mesogen unit in LCM, which can undergo $\pi-\pi$ stacking. With increasing the delay between initiation and LCM addition, the morphology changes from microgels with only a few compartments to microgels with many compartments (Figure 3k). After a 5 min delay of LCM (Figure 3g), the compartments are less defined compared to the microgels with a 4 min delay (Figure 3f). After a 10 min delay, the formation of small secondary particles

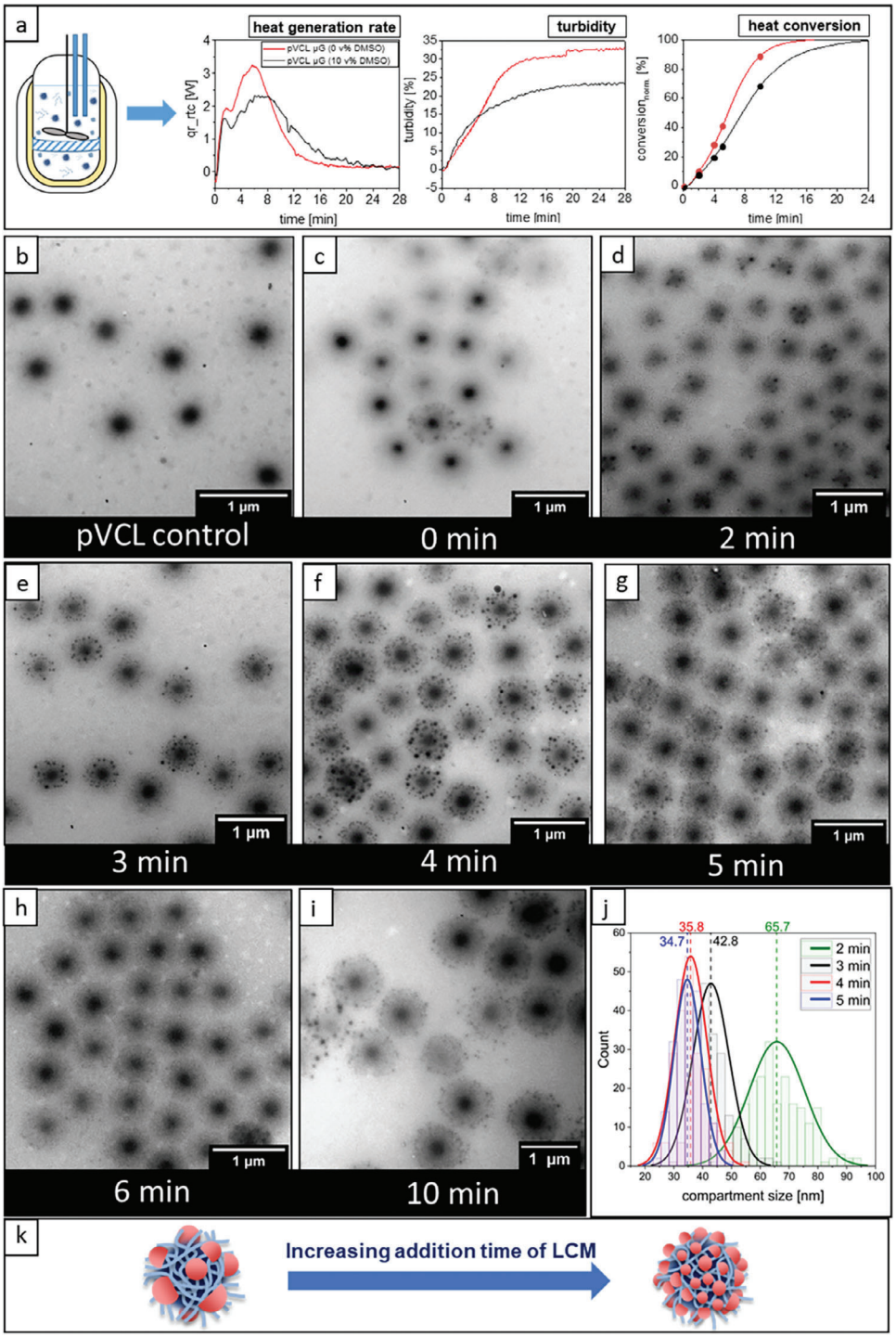


**Figure 3.** a) Heat generation rate, turbidity, and relative conversion obtained from the pVCL microgel synthesis using in-line reaction calorimetry (In the heat conversion graph, the red and black dots represent different LCM addition times used in the subsequent synthesis.); b) TEM images of pVCL microgels; c–i) TEM images of p(VCL-*co*-LCM) microgels synthesized with different addition times of LCM ranging from 0 to 10 min; j) Histograms illustrating the diameters of the compartment sizes in the microgels with 2 to 5 min delayed addition of LCM measured from TEM images using ImageJ. Solid lines indicate the normalized distribution, while dashed lines denote the mean compartment size. k) schematic representation of the microgel structures.

that are not connected to the microgel takes place (Figure 3i). Based on the knowledge we gained from the reaction calorimetry, we assume that this is due to the increasing consumption of VCL during the synthesis and growth of the pVCL precursor microgels. The compartment sizes of the microgels were determined using several TEM images, with LCM delay times ranging from 2 to 5 min. The diameter of ≈200 compartments was measured for each sample. These measurements were presented as histograms (see Figure S5, Supporting Information). Figure 3j shows a normalized distribution that combines all four histograms, with the mean size indicated by a dashed line for each delay time. The results demonstrate a progressive decrease in compartment size diameter, from ≈65.7 nm to 42.8, 35.8, and 34.7 nm, corresponding to LCM delay times of 2, 3, 4, and 5 min, respectively.

Furthermore, a gradual addition of LCM over a span of 20 min was examined using a syringe pump. Various feeding strategies were tested: a) LCM and initiator, b) LCM with 50 wt.% initiator with the remaining 50 wt.% initiator added in a single dose at the beginning of the feeding, and c) LCM only. Nonetheless, this method also leads to the formation of secondary particles, as evidenced by the TEM images depicted in Figure S7 (Supporting Information). NMR and Raman spectroscopy were utilized to assess the LCM within the microgels quantitatively. In quantitative $^1$H-NMR, 1,2,4,5-Tetrachloro-3-nitro-benzene serves as an internal standard in the NMR solvent $CDCl_3$, while for Raman spectroscopy, a calibration curve was determined by the preparation of the homopolymers pVCL and pLCM (Figure S1, Supporting Information). The calculations of both, as well as the synthesis procedure of the homopolymers, can be found in the Supporting Information. All samples had a similar value between 2–3 mol% of polymerized LCM, with the addition after 4 min giving the highest incorporation of LCM (Table S1, Supporting Information). The unreacted LCM precipitated in the reaction solution after some time due to the relatively low concentration of DMSO (5 v%) and was removed by filtration prior to dialysis. However, traces of the monomer remained in the microgels, as confirmed by $^1$H-NMR analysis. (Figure S2, Supporting Information). The yield was gravimetrically determined and ranges from 95 to 86%. A slight decrease is noticeable with increasing delay time (Table S1, Supporting Information). A reason for the decrease in yield could be the agglomeration of colloidally unstable particles, which were also removed from the reaction solution by filtration prior to dialysis. All samples exhibit temperature-responsive behavior, as confirmed by DLS measurements. In the swollen state, the hydrodynamic diameter ranges from 942 to 1200 nm at 20 °C, while in the collapsed state, it varies from 428 to 489 nm at 50 °C (Table S2, Supporting Information).

### 2.3. Influence of the Solvent Concentration

Besides time, the amount of solvent used is a crucial parameter to consider when synthesizing multicompartment microgels. As the previous syntheses were carried out with a minimal amount of 5 v% DMSO, the synthesis of the different delay times of LCM was repeated from Section 2.2 with 10 v% DMSO. A similar trend was observed regarding the formation of LCM domains in microgels. TEM images indicate that the morphology changes from a spherical microgel for batch addition of LCM toward multilope-shaped microgels after delayed LCM addition by 2 and 3 min (Figure S4, Supporting Information). With a 4 min delay of LCM, the microgels showed a raspberry-like shape featuring smaller protrusions at 5 and 10 min delay. However, there is also an increase in the formation of secondary particles that are not connected to the microgels, which are visible in the TEM images (Figure S4, Supporting Information). The quantitative $^1$H-NMR and Raman analyses reveal that the amount of LCM in the microgels increases to 4–5 mol% with higher DMSO content (Table S1, Supporting Information). We assume that, with increasing DMSO amount, the hydrophobic LCM has a much higher tendency to polymerize in the continuous phase, forming secondary particles. At the same time, with less DMSO, the polymerization takes place preferably inside or close to the already existing pVCL precursor microgels. Overall, we observed that with 10 v%, we could fully polymerize the 5 mol% LCM that was used during the synthesis.

To further investigate how the DMSO content influences the formation of secondary particles, we compared 10, 25, and 50 v% DMSO while keeping the LCM ratio fixed at 8 mol% added with a 2 min delay. The TEM images in Figure S12 (Supporting Information) clearly reveal that there is an increased formation of secondary particles. Furthermore, the yield of the microgels decreases as the solvent content increases, from 88% at 10 v% DMSO to 62 v% at 50 v% DMSO (Table S5, Supporting Information). This can be explained by the increased solubility of the formed polymer with higher DMSO content, given that precipitation polymerization relies on the insolubility of the resulting polymer. Therefore, the formation of longer polymer chains is required for the precipitation with increasing amounts of DMSO. For that reason, the DMSO content was set between 5 and 10 v% to avoid secondary particle formation and loss of yield. In general, it should be mentioned that DMSO is a widely used solvent known for its ability to dissolve both polar and nonpolar molecules, including drugs that are otherwise poorly soluble. It is commonly used in pharmaceutical synthesis and drug delivery processes due to its generally accepted nontoxicity at concentrations below 10 v%. However, studies have also reported evidence of toxicity at lower concentrations.[61] In the case of the microgels discussed in this study, DMSO is removed after the synthesis through dialysis, and thus it is not expected to influence their subsequent applications.

### 2.4. Influence of the Monomer Ratio on the Microgel Morphology

In the next set of experiments, the ratio between the two monomers, VCL and LCM, was examined. The proportion of LCM varied between 5 and 30 mol% and was added 2 min after the initiation of polymerization while maintaining the DMSO amount fixed at 5 v%. Surprisingly, the increasing LCM amount in the reaction mixture does not result in its higher loadings in the microgels. For the microgel samples with expected 5, 10, 20, and 30 mol% of LCM, 1.8, 2.6, 3.8, and 2.7 mol% of LCM were experimentally determined via $^1$H-NMR (Table S3, Supporting Information). Accordingly, the yield decreases to 63% with an increasing LCM ratio for the sample targeting a 30 mol% LCM loading (Table S3, Supporting Information). The relatively low

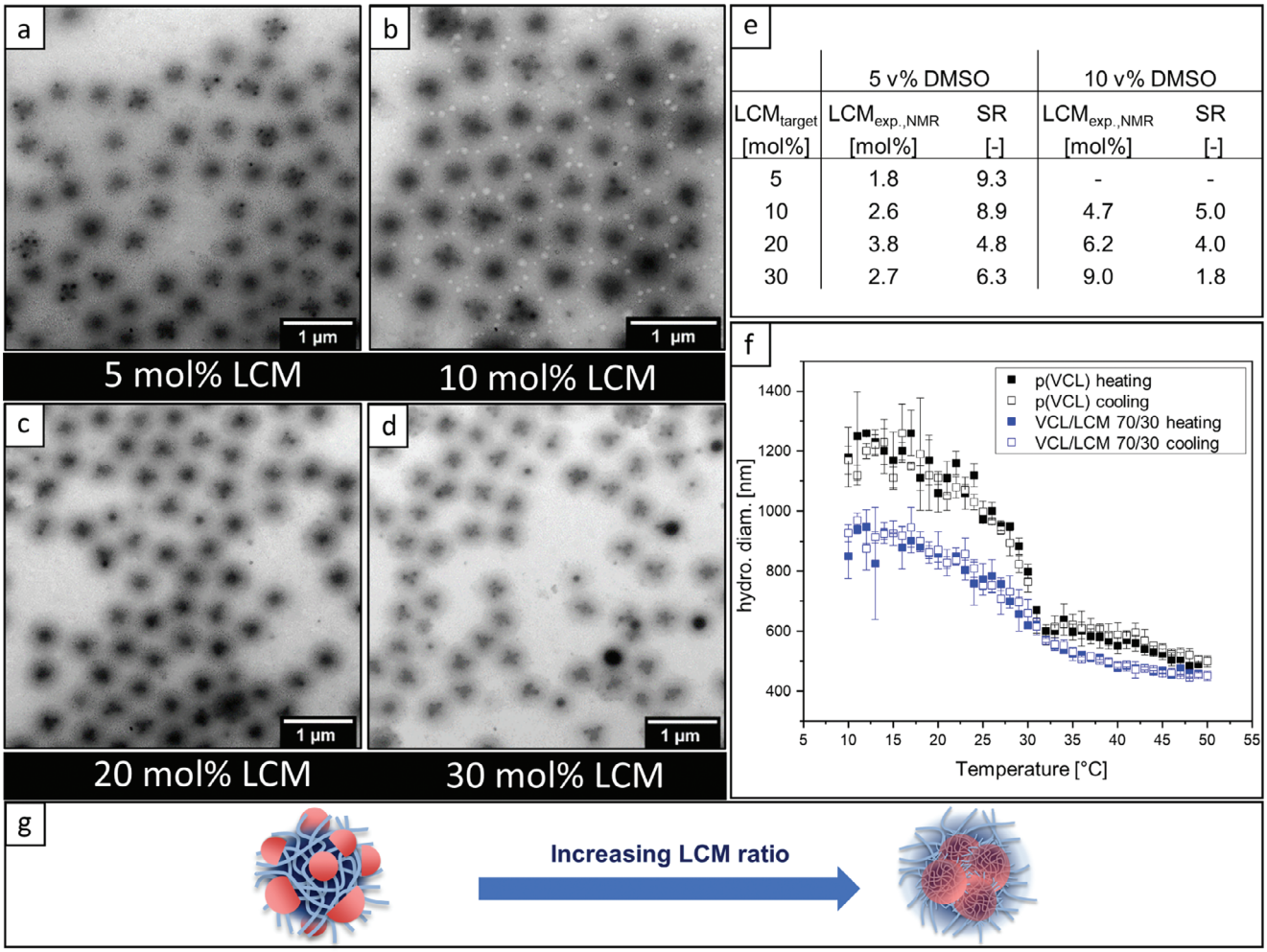


**Figure 4.** a–d) TEM images of synthesized p(VCL-*co*-LCM) microgels targeting 5, 10, 20, and 30 mol% of LCM, respectively; e) swelling ratios (SR) calculated from DLS data (Supporting Information) versus the targeted amount of LCM ($LCM_{target}$) and the experimental amount found by $^1$H-NMR ($LCM_{exp.,\ NMR}$) for 5 and 10 v% DMSO; f) temperature-dependent DLS measurements of pVCL and p(VCL-*co*-LCM) microgels at temperatures from 10 to 50 °C (the filled and hollow squares correspond to the heating and cooling cycles respectively); g) schematic representation of the microgel structure.

incorporation of LCM at higher ratios could arise from the differences in reactivity between the less activated monomer (LCM) and a more activated monomer (VCL). Additionally, the steric hindrance caused by the bulky structure of LCM, which comprises an aromatic mesogen unit and an alkyl chain, contrasts with the relatively compact caprolactam ring of VCL. Consequently, the experimental yield decreases with increasing LCM target during synthesis, as the non-incorporated LCM precipitates, as previously mentioned in Section 2.2. Interestingly, the TEM images presented in **Figure** 4a–d reveal that the morphology of the microgel changes from a raspberry shape (Figure 4a) to an inverse raspberry shape, indicating that LCM-rich domains are localized closer to the microgel core (Figure 4d). The syntheses with different monomer ratios were repeated using 10 v% DMSO, resulting in an increased consumption of LCM, consistent with the observations from the previous section. A maximum of 9 mol% could be quantified by $^1$H-NMR for the microgels targeting 30 mol% LCM (Table S3, Supporting Information). Consistent with previous observations, TEM analysis revealed the presence of a larger number of secondary particles (Figure S2, Supporting Information). An increase in LCM content results in a reduction of the hydrodynamic diameter in the swollen state, decreasing from 939 to 777 nm with 5 v% DMSO and from 994 to 494 nm with 10 v% DMSO. In the collapsed state, the hydrodynamic diameter decreases from 446 to 421 nm and from 501 to 408 nm, respectively (Table S4, Supporting Information). The temperature-dependent DLS measurements show a decrease in the swelling degree of the microgels with LCM compared to pure pVCL microgels (Figure 4f). The swelling ratio (SR), indicating the deformation of the microgels when switching from the swollen to the collapsed state, was calculated from the DLS data at 20 °C and 50 °C (see Equation S2 and Table S4, Supporting Information). As the amount of LCM incorporated during synthesis increases, the SR decreases from 9.3 for microgels with 1.8 mol% LCM to 4.8 for those with 3.8 mol% LCM (Figure 4e). For microgels synthesized using 10 v% DMSO, the SR decreases further to 1.8, corresponding to the incorporation of 9.0 mol% LCM (Figure 4e). The results indicate that an

increase in LCM content within the microgel leads to a decrease in the SR.

### 2.5. Influence of the Reaction Temperature on the Microgel Morphology

The temperature of the reaction plays an important role in precipitation polymerization. We showed in previous work that the size of the formed microgels can be tuned by ramping the temperature.[69] By decreasing the temperature, the decomposition rate of the thermal initiator AMPA is reduced. This leads to a smaller number of primary radicals and fewer nuclei and results in larger microgels. In our case, that also means that there are fewer nuclei centers for the LCM to start polymerization. Additionally, to the initiator decomposition, a lower temperature may promote a more efficient assembly of LC molecules, as the LC phases of LCM are also affected by temperature. The temperature-ramp was achieved by adding the initiator at room temperature before immersing the flask into the oil bath. The LCM ratio was kept constant at 5 mol% with 10 v% DMSO. LCM was added delayed after 4.5 min, which was the time at which the reaction solution started to become visually turbid (**Figure 5**a). By choosing different end temperatures for the temperature-ramp, the microgel shape was varied from dumbbell to multilope shapes. For 70 and 80 °C, similar dumbbell-like structures were generated (Figures 5b and S15 and S17, Supporting Information). For an end temperature of 90 °C, we could observe microgels with 3–5 defined LCM-rich compartments. When applying the temperature-ramp for pVCL microgels without LCM, we observe only spherical microgel structures in TEM for all temperatures (Figure S14, Supporting Information). A higher contrast of the small compartments, displayed by a darker appearance, is observable for microgels synthesized at an end temperature of 90 °C. In Figure 5d,e, the contrast profiles of single particles are visualized by plotting the gray value against the distance where the highest gray value at 200 corresponds to the background. The plot from the dumbbell particle (Figure 5d) reveals variations in the contrast between the two spheres, indicating differences in density and crystallinity as discussed in Section 2.2, and thus suggesting anisotropy in the structure. The same observation applies to the compartments of the multilobe structure (Figure 5e). Similar multilobe structures are known from self-assembled block copolymers to form multicompartment micelles.[70] To verify the structure in the swollen state and to ensure that the microgel morphologies are not influenced by drying and agglomeration effects, additional images of the dumbbell and multilobe structures were taken with cryogenic TEM (cryo-TEM) (Figure 5b,c, right side). The results are consistent with previous dry-state images, indicating that the observed morphologies are not artifacts of the drying process. Overall, the compartments of the p(VCL-*co*-LCM) microgels synthesized using the temperature-ramp method are larger in size compared to those in previously studied microgels prepared through monomer and addition time variation. The compartment size diameters of the microgels were measured analogously to the earlier studies of the delayed LCM addition from TEM images. The normalized distribution indicates that the microgels synthesized with an end temperature of 70 °C are ≈178.7 nm, while the ones with an end temperature of 90 °C are 151.4 nm in diameter (see Figure S16, Supporting Information). However, the incorporation of LCM showed no significant difference compared to microgels synthesized with 10 v% DMSO and a 4 min addition time.

Furthermore, differential scanning calorimetry (DSC) was conducted to investigate the melting of the crystalline moieties in the microgels, which can be observed by determining the melting temperature ($T_m$). This is evidenced by an endothermic peak in the thermogram of the lyophilized p(VCL-*co*-LCM) microgel (Figure S21a, Supporting Information), appearing at a temperature similar to the $T_m$ of pure LCM (Figure S21b, Supporting Information).

### 2.6. Uptake of Hydrophobic Model Substance

A potential application of the compartmentalized microgels presented in this study is the encapsulation of hydrophobic substances, such as drugs that are otherwise insoluble in water. Consequently, Nile Red (NR) was selected as a model substance due to its pronounced hydrophobicity and insolubility in water. This fluorescent dye, with an absorption maximum around $\lambda = 560$ nm, facilitates the monitoring of its uptake into the microgels using UV/vis spectroscopy. Microgels with two different VCL to LCM ratios were chosen for this purpose to monitor the efficiency of different amounts of incorporated LCM. A series of NR concentrations were prepared by adding varying amounts of NR to a stock solution of the respective microgel in ultrapure water ($c$ = 15 mg mL$^{-1}$), covering the range of m(NR)/m(microgel) = 0–7.0 µg mg$^{-1}$. All samples were recorded in the wavelength range of $\nu$ = 800–400 nm. The sample without NR was used as the reference baseline for absorbance measurements and was subtracted from the NR loaded microgel spectra. To enable a quantitative comparison of the intensity of the absorbance maximum, the UV/vis measurements were conducted at a consistent dilution across all samples. The resulting absorbance spectra are depicted in **Figure 6**a,b with 2.5 and 4.3 mol% LCM, respectively. The absorbance at the maximum is plotted against the NR concentration (Figure 6c), and the maximum loading capacity is defined by the amount of NR used for the sample exhibiting the highest absorbance indicated by the dashed line. The maximum NR loading in the microgels corresponds to 0.6 wt.% for the microgel containing 4.3 mol% LCM and 0.4 wt.% for the microgel containing 2.5 mol% LCM. With increasing NR amounts, a decrease in the absorbance is noticeable for both microgels, which can be explained by a loss in colloidal stability, resulting in agglomeration and precipitation of the microgels from the solution. Similar effects have been reported in previous studies with microgels by Belthle et al.[38] Furthermore, for microgels with only VCL as a monomer, an uptake of NR that is close to zero was reported in the literature by Kehren et al., which shows that the hydrophobic model substance cannot be uptaken by conventional microgels.[39]

These experiments provide initial evidence of the unique properties of the microgels and demonstrate the broader applicability of the microgels in potential drug delivery systems.

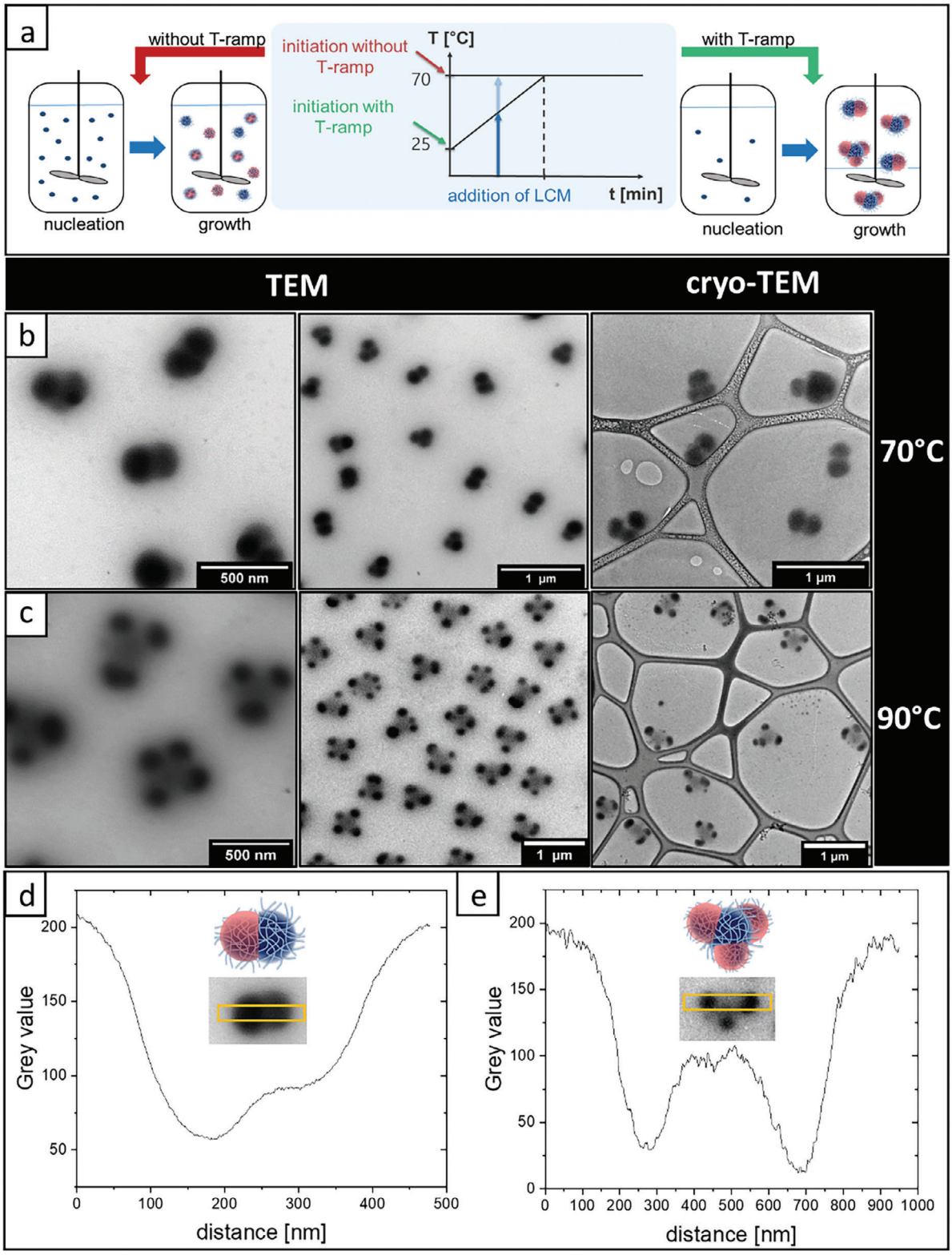


**Figure 5.** a) Schematic representation of the effect of a temperature-ramp on the microgel synthesis; b,c) TEM (left, middle) and cryo-TEM images (right) of synthesized microgels using a *T*-ramp with the end temperature of 70 and 90 °C respectively; Gray value profile from TEM images of single microgels with d) $T_{end}$ = 70 °C and e) $T_{end}$ = 90 °C (performed using Image J software). Included is a schematic representation of the microgel along with a TEM image. The yellow square indicates the region used for applying the gray value profile analysis.

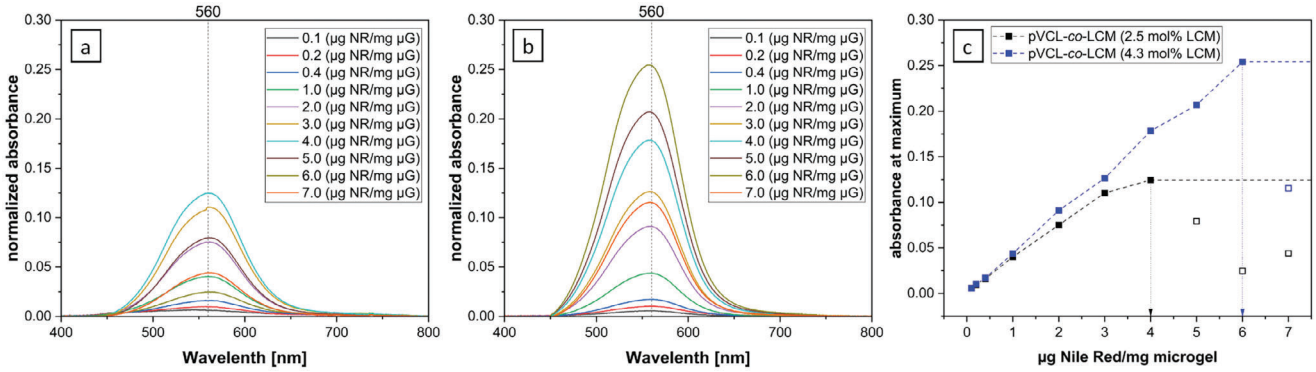


**Figure 6.** Absorbance of Nile Red (NR) loaded samples with different NR amounts measured by UV/vis spectroscopy for p(VCL-*co*-LCM) microgel with a) 2.5 mol% LCM incorporated and b) 4.3 mol% LCM incorporated. c) Depicts the absorbance at the maximum $\lambda = 560$ nm depending on the NR amount for both microgels. The dashed line is a visual guide to the eye and the plateau at the end represents the maximum loading capacity. The unfiled squares represent the samples where agglomeration and precipitation of the microgels reduce the absorbance at 560 nm.

## 3. Conclusion

In this work, we presented the synthesis of novel asymmetric temperature-responsive microgels by copolymerization of *N*-vinylcaprolactam (VCL) and amphiphilic liquid crystalline (LC) monomer 4-methoxybenzoic acid 4-(6-acryloyloxy hexyloxy)phenyl ester (LCM) using precipitation polymerization. We systematically investigated how the addition time of LCM, temperature, solvent concentration, and monomer ratio influence the final microgel morphology. Using $^1$H-NMR- and Raman spectroscopy, the polymerization of both monomers was studied, and the amount of incorporated LCM was quantitatively determined. Using electron microscopy, we investigated the microgel morphologies while the size and temperature-responsive behavior were studied by dynamic light scattering. Our experimental results show that the morphology of the microgels could be tuned to versatile shapes such as raspberry, dumbbell, or multilobe by variation of the reaction parameters. Furthermore, we investigated the uptake of the hydrophobic model substance Nile Red to explore the potential of those microgels as container systems, for example, for hydrophobic drug delivery applications. This template-free bottom-up synthesis approach offers new opportunities for the scalable production of microgels with diverse shapes. Looking out to the future, these complex architectures exhibit unique properties that have to be further studied, as they are promising candidates for applications in targeted drug delivery systems, interfacial chemistry, and applied optics.

## 4. Experimental Section

*Materials*: *N*-vinylcaprolactam (VCL, 98%, Sigma-Aldrich) was purified by distillation under vacuum and recrystallization from *n*-hexane before usage. The liquid crystalline (LC) monomer 4-methoxybenzoic acid 4-(6-acryloyloxy hexyloxy)phenyl ester (LCM, 97%, Synthon Chemicals), the cross-linker *N,N′*-methylenebisacrylamide (BIS, 99%, Sigma-Aldrich) and the initiator 2,2–azobis(*N*-methylpropionamidine) dihydrochloride (AMPA, 97%, Sigma-Aldrich) were used as received. Nile Red (NR, ≤95%, Thermo Fisher Scientific) was dissolved in acetone/tetrahydrofuran (THF) (2:1, c = 0.3 mg mL$^{-1}$) before use. Dimethyl sulfoxide for microgel synthesis was of analytical grade (DMSO, 100%, VWR Chemicals).

*Microgel Synthesis*: The microgels were synthesized using a semi-batch precipitation polymerization. The following procedure was exemplary for a synthesis with 5 mol% LCM and 5 v% DMSO. VCL (420.8 mg, 3.02 mmol) and the cross-linker BIS (6.18 mg, 0.04 mmol) were dissolved in HPLC-grade water (18 mL). LCM (63.4 mg, 0.16 mmol) and the initiator AMPA were dissolved separately in DMSO (1 mL) and HPLC-grade water (1 mL), respectively. All three solutions were purged with nitrogen for 30 min. The reaction was started by the addition of the initiator solution at 70 °C. The LCM solution was added with a 0 to 20 min delay to the synthesis. After 6 h, the reaction was stopped by cooling to room temperature while the stirring was continued overnight. The synthesized microgels were dialyzed against deionized water for 5 days using dialysis membranes (MWCO 12–14 kDa) to remove DMSO and residues from unreacted monomer and cross-linker. After lyophilization, the product was obtained as a white powder. The LCM content was determined via Raman spectroscopy and $^1$H-NMR.

*Microgel Synthesis with Temperature-Ramp*: For the temperature-ramped synthesis, the solutions were prepared equally. In contrast to the conventional semi-batch synthesis, the initiator solution was added to the reaction solution at room temperature. Afterward, the round bottom flask was immersed in the oil bath, which was set between 70 and 90 °C. The LCM solution was added after 4.5 min. The purification of obtained microgels was similar to the procedure described above.

*Loading of Hydrophobic Model Substance Nile Red into Microgels*: To explore the uptake efficiency of the microgels with a hydrophobic substance, the water-insoluble fluorescent dye Nile Red served as a model compound. The experiments were performed with two VCL to LCM compositions (2.5 and 4.3 mol% incorporated LCM) following an established protocol.[39] The microgel dispersion was diluted to $c = 15$ mg mL$^{-1}$ using HPLC-grade water from the original dispersion after dialysis. The concentration of the original solution was previously determined by lyophilization. Nile Red was dissolved using a mixture of acetone/THF of 2:1 (v/v) with a concentration of 0.3 mg mL$^{-1}$. The dye solution was added to 0.5–1.0 mL of the aqueous microgel dispersion, obtaining Nile red ratios of m(Nile Red)/m(microgel) = 0–7 µg mg$^{-1}$. The sample without added dye served as the reference sample. The samples were allowed to equilibrate for 24 h in an open vial, ensuring sedimentation of free Nile Red not taken up by the microgels and evaporation of the organic solvent. The samples were diluted with a dilution of 1:31 (62.5 µL of sample with 1937 µL water).

*Raman Spectroscopy*: Raman spectroscopy was used to detect the incorporation of LCM into the microgel network on a Bruker RFS 100/S Raman spectrometer with an Nd:YAG laser ($k$ = 1064 nm). Measurements

were performed with a spectral resolution of 4 $cm^{-1}$, power of 200 mW, and 1000 scans. For the measurements and the analysis, the software OPUS 4.0 was used. Baseline corrections were performed.

*Electron Microscopy*: For Scanning Electron and Scanning Transmission Electron Microscopy (SEM/STEM) measurements, an ultra-high-resolution SU-9000 microscope by Hitachi was used. The electron energy was set between 20–30 kV, and the magnification was between ×60000 and ×180000. The mode was varied between the Bright Fields STEM (BF-STEM) and Scanning Electron (SE) modes. For Transmission Electron Microscopy (TEM) measurements, a Zeiss Libra 120 device was used. The emission current was between 5–10 µA, the electron energy was set to 120 kV, and the magnification was chosen between ×4000 and ×10000. For both methods, samples were diluted with HPLC-grade water with concentrations between 0.7–1.0 mg $mL^{-1}$, which were priorly determined by lyophilization. A droplet of 7 µL was placed onto a carbon-coated copper grid (400 Mesh), while the excess liquid was absorbed with filter paper. The sample was set to dry for several hours so the solvent could evaporate before the measurement.

For cryogen transmission electron microscopy (cryo-TEM) measurements, a high-resolution JEM-2100Plus microscope by JEOL was used. The acceleration voltage was set to 200 kV, and the magnification was chosen between ×8000 and ×15000. The microgels were diluted, as stated previously. The dispersions were vitrified on lacey carbon film-coated copper grids using an EM GP2 Automatic Plunge Freezer.

*Dynamic Light Scattering*: Dynamic light scattering (DLS) was performed to determine the hydrodynamic diameter and the size distribution of the microgels using a Zetasizer Ultra by Malvern Panalytical and analyzed using the software ZS Xplorer. All samples were diluted in HPLC-grade water and transferred into a disposable capillary cell of the type DTS0012. The samples were measured at an angle of 90° (sidescatter) at temperatures of 20 or 50 °C four times. For the temperature-dependent measurements, the temperature was set from 5 to 50 °C (and backward). The hydrodynamic diameter was determined at every single degree three times, using the mean peak values from the intensity-weighted distribution.

*Reaction Calorimetry*: Calorimetric measurements were executed using an RC1e reaction calorimeter from Mettler Toledo. The reactor, an AP01-0.5-RTCal 500 mL 3-wall reactor, was equipped with a baffle, a Hastelloy@ stirrer, and a Turbido turbidity probe from Solvias. The measurements were performed in the isothermal mode. Thereby, the desired reaction temperature ($T_r$) was set to a constant value, while the temperature of the jacket ($T_j$) was changed automatically to keep the $T_r$ at the desired temperature. The data evaluation was performed with the software iControl RC1e 5.3. The monomers VCL and the cross-linker BIS were dissolved in 150 mL of deionized water and heated to 70 °C while stirring at 300 rpm. The solution was degassed for 30 min. Before the initiation of the reaction, the heat flow was equilibrated for 90 min to generate a stable baseline. The initiator was added dry, and the synthesis was carried out for 90 min. The exact compositions of the synthesis can be found in Table S9 (Supporting Information).

*NMR Spectroscopy*: $^1$H-NMR spectra of the microgels were recorded on a Bruker AV400 Spectrometer at 400 MHz. For all measurements, deuterated chloroform ($CDCl_3$, chemical shift $\delta$ H = 7.26 ppm) was used as a solvent. For the quantitative NMR measurements, 1,2,4,5-Tetrachloro-3-nitro-benzene was used as an internal standard. The NMR spectra, as well as the calculations for the quantitative determination, can be found in the Supporting Information.

*UV/Vis Spectroscopy*: The UV/Vis measurements of the absorbance of the Nile Red loaded microgels were performed using a JASCO V-780 spectrophotometer in the wavelength region of $\lambda$ = 800–400 nm. The device was operated using a scan speed of 200 nm $min^{-1}$, a data interval of 0.5 nm, and a NIR bandwidth of 1.0 nm. A sample without added dye was measured as a reference sample and subtracted as a baseline from the Nile Red loaded samples. The spectra were normalized to the means of the end values (800 and 400 nm) in each microgel concentration series, respectively.

*Differential Scanning Calorimetry*: Differential scanning calorimetry (DSC) measurements were performed using a DSC 8500 differential scanning calorimeter from Perkin Elmer, featuring a CLN2 Controlled Liquid Nitrogen Accessory, a fiber-optic illuminator, and an OmniCure S2000 light source. Approximately 30 mg of the lyophilized microgel was pressed into a pallet and transferred into an aluminum pan. In the case of the monomer, ≈5 mg was used and pressed directly into the aluminum pan. Measurements were performed under an $N_2$ atmosphere at temperatures between 0 to 140 °C, applying a heating rate of 10 K $min^{-1}$.

## Supporting Information

Supporting Information is available from the Wiley Online Library or from the author.

## Acknowledgements

This work was performed as a part of project B4 of the CRC 985 "Functional Microgels and Microgel Systems" funded by Deutsche Forschungsgemeinschaft (DFG). The authors gratefully acknowledge Inga Litzen for performing AFM measurements and Stefan Hauk for recording STEM images.

Open access funding enabled and organized by Projekt DEAL.

## Conflict of Interest

The authors declare no conflict of interest.

## Data Availability Statement

The data that support the findings of this study are available from the corresponding author upon reasonable request.

## Keywords

asymmetric colloids, liquid crystals, precipitation polymerization, self-assembly, thermoresponsive microgels

Received: November 6, 2024
Revised: December 20, 2024
Published online:

[1] E. Poggi, J. F. Gohy, *Colloid Polym. Sci.* **2017**, *295*, 2083.
[2] S. C. Glotzer, M. J. Solomon, *Nat. Mater.* **2007**, *6*, 557.
[3] J. A. Champion, Y. K. Katare, S. Mitragotri, *JCP* **2007**, *121*, 3.
[4] J. Hu, S. Zhou, Y. Sun, X. Fang, L. Wu, *Chem. Soc. Rev.* **2012**, *41*, 4356.
[5] B. J. Park, T. Brugarolas, D. Lee, *Soft Matter* **2011**, *7*, 6413.
[6] X. Yan, F. Wang, B. Zheng, F. Huang, *Chem. Soc. Rev.* **2012**, *41*, 6042.
[7] F. A. Plamper, W. Richtering, *Acc. Chem. Res.* **2017**, *50*, 131.
[8] A. Pich, A. Tessier, V. Boyko, Y. Lu, H. J. P. Adler, *Macromolecules* **2006**, *39*, 7701.
[9] R. Pelton, *Adv. Colloid Interface Sci.* **2000**, *85*, 1.
[10] A. Garcia, M. Marquez, T. Cai, R. Rosario, Z. Hu, D. Gust, M. Hayes, S. A. Vail, C. D. Park, *Langmuir* **2007**, *23*, 224.
[11] T. Hoare, R. Pelton, *Macromolecules* **2004**, *37*, 2544.
[12] D. Duracher, F. Sauzedde, A. Elaïssari, C. Pichot, L. Nabzar, *Colloid Polym. Sci.* **1998**, *276*, 920.
[13] A. Suzuki, T. Tanaka, *Nature* **1990**, *346*, 345.
[14] C. H. Hofmann, F. A. Plamper, C. Scherzinger, S. Hietala, W. Richtering, *Macromolecules* **2013**, *46*, 523.

[15] Y. Lu, S. Proch, M. Schrinner, M. Drechsler, R. Kempe, M. Ballauff, *J. Mater. Chem.* **2009**, *19*, 3955.
[16] V. C. Lopez, J. Hadgraft, M. J. Snowden, *Int. J. Pharm.* **2005**, *292*, 137.
[17] J. K. Oh, R. Drumright, D. J. Siegwart, K. Matyjaszewski, *Prog. Polym. Sci.* **2008**, *33*, 448.
[18] C. C. Cutright, J. L. Harris, S. Ramesh, S. A. Khan, J. Genzer, S. Menegatti, C. C. Cutright, J. L. Harris, S. Ramesh, S. A. Khan, J. Genzer, S. Menegatti, *Adv. Funct. Mater.* **2021**, *31*, 2104164.
[19] M. Kather, M. Skischus, P. Kandt, A. Pich, G. Conrads, S. Neuss, *Angew. Chem., Int. Ed.* **2017**, *56*, 2497.
[20] Q. Feng, D. Li, Q. Li, X. Cao, H. Dong, *Bioact. Mater.* **2022**, *9*, 105.
[21] Y. Wang, L. Guo, S. Dong, J. Cui, J. Hao, *Adv. Colloid Interface Sci.* **2019**, *266*, 1.
[22] A. Laukkanen, S. K. Wiedmer, S. Varjo, M. L. Riekkola, H. Tenhu, *Colloid Polym. Sci.* **2002**, *280*, 65.
[23] H. Vihola, A. Laukkanen, L. Valtola, H. Tenhu, J. Hirvonen, *Biomaterials* **2005**, *26*, 3055.
[24] J. Liu, A. Debuigne, C. Detrembleur, C. Jérôme, *Adv. Healthcare Mater.* **2014**, *3*, 1941.
[25] G. Agrawal, R. Agrawal, G. Agrawal, R. Agrawal, *Small* **2018**, *14*, 1801724.
[26] A. Pich, W. Richtering, *Chemical Design of Responsive Microgels*, Springer, Berlin Heidelberg, **2010**.
[27] L. P. B. Guerzoni, J. C. Rose, D. B. Gehlen, A. Jans, T. Haraszti, M. Wessling, A. J. C. Kuehne, L. De Laporte, *Small* **2019**, *15*, 1900692.
[28] S. Seiffert, *Macromol. Rapid Commun.* **2012**, *33*, 1286.
[29] S. Keller, R. Dekkers, G. X. Hu, M. Tollemeto, M. Morosini, A. Keskin, D. A. Wilson, *React. Funct. Polym.* **2021**, *167*, 105012.
[30] D. L. Braunmiller, S. Babu, D. B. Gehlen, M. Seuß, T. Haraszti, A. Falkenstein, J. Eigen, L. De Laporte, J. J. Crassous, *Adv. Funct. Mater.* **2022**, *32*, 202202430.
[31] S. H. Jung, S. Bulut, L. P. B. Busca Guerzoni, D. Günther, S. Braun, L. De Laporte, A. Pich, *J. Colloid Interface Sci.* **2022**, *617*, 409.
[32] H. J. M. Wolff, J. Linkhorst, T. Göttlich, J. Savinsky, A. J. D. Krüger, L. De Laporte, M. Wessling, *Lab Chip* **2020**, *20*, 285.
[33] F. Grabowski, V. S. Petrovskii, F. Fink, D. E. Demco, S. Herres-Pawlis, I. I. Potemkin, A. Pich, *Adv. Sci.* **2022**, *9*, 202204853.
[34] W. Xu, A. Rudov, A. Oppermann, S. Wypysek, M. Kather, R. Schroeder, W. Richtering, I. I. Potemkin, D. Wöll, A. Pich, *Angew. Chem., Int. Ed.* **2020**, *59*, 1248.
[35] J. A. Champion, Y. K. Katare, S. Mitragotri, *J. Controlled Release* **2007**, *121*, 3.
[36] P. Lagarrigue, F. Moncalvo, F. Cellesi, *Pharmaceutics* **2023**, *15*, 32.
[37] D. S. T. Hsieh, W. D. Rhine, R. Langer, *J. Pharm. Sci.* **1983**, *72*, 17.
[38] T. Belthle, D. E. Demco, A. Pich, *Macromolecules* **2022**, *55*, 844.
[39] D. Kehren, C. M. Lopez, S. Theiler, H. Keul, M. Möller, A. Pich, *Polymer* **2019**, *172*, 283.
[40] D. Demus, J. Goodby, G. W. Gary, H. W. Spiess, V. Vill, *Handbook of Liquid Crystals*, Wiley-VCH, Weinheim **1998**.
[41] J. Uchida, B. Soberats, M. Gupta, T. Kato, *Adv. Mater.* **2022**, *34*, 202109063.
[42] V. K. Thakur, M. R. Kessler, *Liquid Crystalline Polymers Volume 1-Structure and Chemistry*, Springer, Cham **2016**.
[43] A. M. Martinez, M. K. McBride, T. J. White, C. N. Bowman, *Adv. Funct. Mater.* **2020**, *30*, 202003150.
[44] H. M. Van Der Kooij, D. J. Broer, D. Liu, J. Sprakel, *ACS Appl. Mater. Interfaces* **2020**, *12*, 19927.
[45] D. Liu, C. W. M. Bastiaansen, J. M. J. Den Toonder, D. J. Broer, *Macromolecules* **2012**, *45*, 8005.
[46] D. Martella, S. Nocentini, D. Antonioli, M. Laus, D. S. Wiersma, C. Parmeggiani, *Polymers* **2019**, *11*, 1644.
[47] D. Martella, P. Paoli, J. M. Pioner, L. Sacconi, R. Coppini, L. Santini, M. Lulli, E. Cerbai, D. S. Wiersma, C. Poggesi, C. Ferrantini, C. Parmeggiani, *Small* **2017**, *13*, 201702677.
[48] H. Shahsavan, A. Aghakhani, H. Zeng, Y. Guo, Z. S. Davidson, A. Priimagi, M. Sitti, *Proc. Natl. Acad. Sci. USA* **2020**, *117*, 5125.
[49] X. Liu, Y. Xu, J. P. A. Heuts, M. G. Debije, A. P. H. J. Schenning, *Macromolecules* **2019**, *52*, 8339.
[50] A. Belmonte, T. Bus, D. J. Broer, A. P. H. J. Schenning, *ACS Appl. Mater. Interfaces* **2019**, *11*, 14376.
[51] H. P. C. Van Kuringen, D. J. Mulder, E. Beltran, D. J. Broer, A. P. H. J. Schenning, *Polym. Chem.* **2016**, *7*, 4712.
[52] M. Vennes, S. Martin, T. Gisler, R. Zentel, *Macromolecules* **2006**, *39*, 8326.
[53] T. Bera, E. J. Freeman, J. A. McDonough, R. J. Clements, A. Aladlaan, D. W. Miller, C. Malcuit, T. Hegmann, E. Hegmann, *ACS Appl. Mater. Interfaces* **2015**, *7*, 14528.
[54] R. K. Shaha, A. H. Torbati, C. P. Frick, *J. Appl. Polym. Sci.* **2021**, *138*, 50136.
[55] D. R. Cairns, N. S. Eichenlaub, G. P. Crawford, *Mol. Crys. Liq. Cost.* **2000**, *352*, 275.
[56] D. R. Cairns, M. Sibulkin, G. P. Crawford, *Appl. Phys. Lett.* **2001**, *78*, 2643.
[57] X. Liu, M. G. Debije, J. P. A. Heuts, A. P. H. J. Schenning, *Chem. - Eur. J.* **2021**, *27*, 14168.
[58] X. Liu, X. Pan, M. G. Debije, J. P. A. Heuts, D. J. Mulder, A. P. H. J. Schenning, *Soft Matter* **2020**, *16*, 4908.
[59] S. R. Lee, E. Reichmanis, M. Srinivasarao, *ACS Macro Lett.* **2022**, *11*, 96.
[60] Y. Liu, L. Xing, Q. Zhang, Q. Mu, P. Liu, K. Chen, L. Chen, X. Zhang, K. Wang, Y. Wei, *Colloid Polym. Sci.* **2016**, *294*, 617.
[61] J. Galvao, B. Davis, M. Tilley, E. Normando, M. Duchen, M. Cordeiro, *FASEB J.* **2014**, *3*, 1317.
[62] X. Yin, H. Dong, S. Wang, Y. Liang, W. Zhang, N. Gao, X. Liu, X. Wang, G. Li, *Macromol. Chem. Phys.* **2018**, *219*, 201800113.
[63] S. Iamsaard, E. Anger, S. J. Aßhoff, A. Depauw, S. P. Fletcher, N. Katsonis, *Angew. Chem., Int. Ed.* **2016**, *55*, 9908.
[64] T. Belthle, D. E. Demco, A. Pich, *Macromolecules* **2022**, *55*, 844.
[65] M. Kather, F. Ritter, A. Pich, *Chem. Eng. J.* **2018**, *344*, 375.
[66] F. Jung, A. Ksiazkiewicz, A. Mhamdi, A. Pich, A. Mitsos, *Chem. Eng. J.* **2019**, *378*, 121740.
[67] F. A. L. Janssen, M. Kather, L. C. Kröger, A. Mhamdi, K. Leonhard, A. Pich, A. Mitsos, *Ind. Eng. Chem. Res.* **2017**, *56*, 14545.
[68] G. H. Michler, W. Lebek, *Polymer Morphology: Principles, Characterization, and Processing*, Wiley, Hoboken, NJ USA **2016**, 3.
[69] A. N. Ksiazkiewicz, L. Bering, F. Jung, N. A. Wolter, J. Viell, A. Mitsos, A. Pich, *Chem. Eng. J.* **2020**, *379*, 122293.
[70] A. H. Gröschel, F. H. Schacher, H. Schmalz, O. V. Borisov, E. B. Zhulina, A. Walther, A. H. E. Müller, *Nat. Commun.* **2012**, *3*, 710.